

# The Interrelationship of Atmospheric Correction of Reflectances and Surface BRDF Retrieval: A Sensitivity Study

Baoxin Hu, Wolfgang Lucht, and Alan H. Strahler, *Member, IEEE*

**Abstract**—This paper systematically studies the interrelationship between surface bidirectional reflectance distribution function (BRDF) retrieval and atmospheric correction. The study uses the atmospheric correction scheme of the Moderate Resolution Imaging Spectroradiometer (MODIS) and angular sampling expected for MODIS and the Multiangle Imaging SpectroRadiometer (MISR) for different land cover types and optical depths of aerosols. The results show the following two points.

- 1) Even for a nonturbid atmosphere, the assumption of a Lambertian surface in atmospheric correction causes relative errors in the retrieved surface reflectances that average from 2 to 7% in the red and near-infrared bands, with worst cases showing errors of up to about 15% for turbid conditions. Consequently, it is necessary for improved accuracy to consider surface anisotropy in atmospheric correction.
- 2) Surface BRDF retrieval and atmospheric correction can be coupled in a converging iteration loop that improves the quality of atmospheric correction and subsequent BRDF retrievals. For example, performing two steps of the iteration loop is already sufficient to obtain mean relative errors of less than 1% in the retrieved surface reflectances even for an atmospheric aerosol optical depth of 0.4.

As BRDF retrieval accuracies improve, so do bihemispherical albedo retrieval accuracies, with mean relative errors being 1–5% when using a Lambertian assumption and less than 1% after two iteration steps.

**Index Terms**—Atmospheric correction, bidirectional reflectance distribution function, Earth Observing System (EOS), land surface albedo, moderate resolution imaging spectroradiometer (MODIS).

## I. INTRODUCTION

THE SIGNALS received by a space-based or airborne remote sensor in the solar spectral range do not directly characterize the reflectance of surface objects, due to effects of the intervening atmosphere. Thus, it is necessary to re-

move atmospheric effects in most land surface remote-sensing applications. Atmospheric effects on upward radiance for a cloudless sky can be computed as the solution to a well-known atmospheric radiative transfer (RT) equation (see, for example, [1] for an introduction). The reflectance properties of the surface provide a lower boundary condition for this equation and are thus required for solving it. In the most general case, a nonuniform and non-Lambertian boundary surface has to be assumed. Work by Case *et al.* [2] indicates that, if the boundary condition is appropriately specified, atmospheric RT may be rigorously decoupled from the transfer within the surface objects.

However, the required reflectance properties of the boundary surface can, in turn, only be retrieved from remotely sensed data after the removal of atmospheric effects, i.e., after the atmospheric transfer problem has been solved. This poses an interdependence problem for surface reflectance retrieval and atmospheric correction of remotely sensed data, which is the topic of this paper.

For example, when the data acquired by a remote-sensing satellite are atmospherically corrected for studies of the surface, the following questions require an answer. Can a Lambertian surface be assumed in atmospheric correction? What error is incurred if the Lambertian assumption is made? How does this error depend on aerosol optical depth, land cover type, and observation geometry? If the instrument in question does not have multiangular capabilities, and a non-Lambertian surface is to be assumed, is it sufficient to work with approximate bidirectional reflectance distribution functions (BRDF's)? In applications in which bidirectional reflectance models are inverted to derive land surface albedo, and the atmospheric correction scheme assumed a Lambertian surface, the question is what errors occur in the BRDF retrieved, and hence, in the albedo derived from the BRDF. This study strives to investigate these questions and to give a quantitative assessment of the atmospheric correction—surface BRDF interdependence problem.

## II. BACKGROUND

In practical applications, the atmosphere–surface scattering interdependence problem is resolved by most researchers by assuming a strongly simplified form of the surface condition. Atmospheric correction methods usually assume that

Manuscript received June 16, 1997; revised May 28, 1998. This work was supported by NASA under Grant NAS5-31369.

B. Hu was with the Department of Geography and the Center for Remote Sensing, Boston University, Boston, MA 02215 USA. She is now with York University, Toronto, Ont., Canada.

A. H. Strahler is with the Department of Geography and the Center for Remote Sensing, Boston University, Boston, MA 02215 USA.

W. Lucht was with the Department of Geography and the Center for Remote Sensing, Boston University, Boston, MA 02215 USA. He is now with the Potsdam-Institut für Klimafolgenforschung (PIK), D-14412 Potsdam, Germany (e-mail: wlucht@pik-potsdam.de).

Publisher Item Identifier S 0196-2892(99)00838-4.

the surface is uniform and Lambertian [3]–[5]. However, this assumption may lead to substantial errors in the surface reflectance retrieved from top-of-atmosphere (TOA) radiances [6], [7]. The atmospheric correction scheme to be employed for NASA’s EOS AM-1 Moderate Resolution Imaging Spectroradiometer (MODIS) couples atmospheric correction and surface reflectance properties specified in form of integrals of the BRDF by performing an iteration loop. In this scheme, atmospheric correction is first performed on MODIS observations under the assumption of a uniform, isotropic surface BRDF in the form of a Lambertian constant. The reflectances found are then used to retrieve a new, non-Lambertian BRDF, and atmospheric correction is updated based on the new BRDF [7].

In theory, this problem of specifying the correct boundary condition at the atmosphere–surface interface is eliminated when a coupled system of atmosphere and earth surface is considered for the RT analysis. A single RT model that includes RT in the atmosphere as well as at the earth’s surface is used to provide solutions for the coupled system. At present, such models have been developed for horizontally homogeneous vegetation canopies [8], [9]. However, solving the coupled RT equation is rather complicated, requiring many approximations and a large amount of calculation [1]. The number of parameters involved is likely to be too large for realistic stable inversions of remote-sensing data. Also, RT theory is not in all cases the most suitable description for land surface scattering, tending to neglect geometric shadowing effects (*cf.*, [10]).

In this paper, we focus on atmospheric correction methods that decouple the atmospheric RT from that within surface objects. The important questions for this class of atmospheric correction methods are whether it is necessary to take surface anisotropic reflectance properties into consideration, how large the effect is if they are neglected, and how to practically include them in retrieval algorithms.

The work of Lee and Kaufman [6] shows that even for a nonturbid atmosphere the assumption of a Lambertian surface leads to noticeable errors in predicted upward radiance in the backscattering portion of the hemisphere, especially for large solar zenith angles. Their research is based on a savanna data set [11]. Vermote *et al.* [7] analyze the effect of surface anisotropic reflectances on atmospheric correction by using a Hapke BRDF model [12] in which the model parameters are determined by fitting a field-measured directional reflectance data set of a plowed field [13]. Their results show that a surface BRDF adequate for use in atmospheric correction can be retrieved through a preliminary atmospheric correction assuming a Lambertian surface. The iteration they suggest arrives at much smaller errors in the surface reflectances than if the Lambertian-based solution had directly been adopted to provide the corrected reflectances. For example, the error is reduced from 10–15% to 2–3% for an aerosol optical depth of 0.23.

We have conducted similar research, using a Ross-Thick/Li-Sparse BRDF model to simulate the BRDF of three different land cover types, and arrived at similar results. A single iteration of a coupled surface BRDF retrieval and atmospheric

correction iteration loop reduced the error to a range from 0.4 to 6.2%. These research results indicate the necessity of taking surface BRDF into account in atmospheric correction.

In spite of these results, the impact of surface BRDF effects on the accuracy of atmospheric correction, and, vice versa, the accuracy of surface BRDF retrieval given an atmospheric correction method requiring assumptions about surface reflectance, is currently not systematically explored. The existing work is limited to demonstrating specific cases over limited land cover types and for limited angular sampling distributions. Therefore, it is hard to draw general conclusions about the errors made or the accuracies to be expected.

In this study, we systematically analyze the interrelationship between surface BRDF retrieval and atmospheric correction by investigating the sensitivity of surface reflectance retrieved from atmospheric correction to the surface reflectance properties used in that correction. We focus on the atmospheric correction method and the angular sampling patterns for the combined EOS AM-1 MODIS and MISR instruments, as surface BRDF effects will routinely be taken into account for the first time in the atmospheric correction for these instruments. We also investigate how albedo retrieval accuracies from BRDF inversions of atmospherically corrected multiangular reflectances are affected by the assumptions about the surface made in the correction method.

### III. THEORETICAL BASIS AND SIMULATION DATA

#### A. Atmospheric Correction Theory

In the atmospheric correction algorithm for MODIS, developed by Vermote *et al.* [7], the reflectances at the TOA for the visible and near-infrared bands are expressed as the following equation. Using their notation

$$\begin{aligned} \rho_{\text{toa}}(\mu_s, \mu_v, \phi) &= \rho_0 + e^{-\tau/\mu_v} e^{-\tau/\mu_s} \rho_s(\mu_s, \mu_v, \phi) \\ &\quad + e^{-\tau/\mu_v} t_d(\mu_s) \bar{\rho} + e^{-\tau/\mu_s} t_d(\mu_v) \bar{\rho}' \\ &\quad + t_d(\mu_s) t_d(\mu_v) \bar{\bar{\rho}} \\ &\quad + \frac{(e^{-\tau/\mu_s} + t_d(\mu_s))(e^{-\tau/\mu_v} + t_d(\mu_v)) S(\bar{\rho})^2}{1 - S\bar{\rho}} \end{aligned} \quad (1)$$

where  $\rho_{\text{toa}}$  is the reflectance at the TOA;  $\rho_0$  is the intrinsic atmospheric reflectance (path reflectance);  $\rho_s$  is the surface reflectance;  $S$  is the reflectance of the atmosphere for isotropic light entering it from the surface;  $\mu_s$  is the cosine of the solar zenith angle;  $\mu_v$  is the cosine of the view zenith angle;  $\phi$  is the relative azimuth between the sun and view directions;  $e^{-\tau/\mu_s}$  and  $t_d(\mu_s)$  are the downward direct and diffuse transmittances of the atmosphere along the path of the incoming solar beam;  $e^{-\tau/\mu_v}$  and  $t_d(\mu_v)$  are the upward direct and diffuse transmittances of the atmosphere in the viewing direction;  $\tau$  is the optical depth of the atmosphere; and  $\bar{\rho}$ ,  $\bar{\rho}'$ , and  $\bar{\bar{\rho}}$  are the surface hemispherical–directional, directional–hemispherical, and hemispherical–hemispherical reflectances (albedos), respectively. These latter terms, also called coupling terms, couple the atmospheric RT with the surface reflectance prop-

erties. They are defined as follows [7]:

$$\begin{aligned} \bar{\rho}(\mu_s, \mu_v, \phi) &= \frac{\int_0^{2\pi} \int_0^1 \mu L_{\downarrow}(\mu_s, \mu, \phi') \rho_s(\mu_s, \mu_v, \phi' - \phi) d\mu d\phi'}{\int_0^{2\pi} \int_0^1 \mu L_{\downarrow}(\mu_s, \mu, \phi') d\mu d\phi'} \end{aligned} \quad (2)$$

$$\bar{\rho}'(\mu_s, \mu_v, \phi) = \bar{\rho}(\mu_v, \mu_s, \phi) \quad (3)$$

$$\begin{aligned} \bar{\bar{\rho}} &= \frac{\int_0^1 \int_0^{2\pi} \int_0^1 \rho_s(\mu, \mu', \phi) \mu \mu' d\mu d\mu' d\phi}{\int_0^1 \int_0^{2\pi} \int_0^1 \mu \mu' d\mu d\mu' d\phi} \end{aligned} \quad (4)$$

where  $L_{\downarrow}(\mu_s, \mu, \phi')$  is the downwelling diffuse irradiance with the sun at  $\mu_s$ . Reciprocity of the BRDF is assumed in (3), otherwise the directional-hemispherical integral over the viewing hemisphere has to be calculated separately.

From these equations, we may note that, given atmospheric optical parameters and estimates of the surface reflectance, the coupling terms (2)–(4) can be calculated, allowing the atmospherically corrected actual surface reflectances to be obtained from observed values of  $\rho_{\text{toa}}$  by solving (1). Operationally, initial estimates of surface reflectance may be taken either from *a priori* knowledge of surface reflectance properties or an independent surface reflectance data product, for example, that for a previous time period. Surface reflectance may, for example, be computed through a BRDF model describing the bidirectional reflectances of the surface through specified parameters. To give more weight to the actual observations than to the estimated surface BRDF used in the calculation of the coupling terms, Vermote *et al.* [7] suggest to modify (1) as follows:

$$\begin{aligned} \rho_{\text{toa}} &= \rho_o + e^{-\tau/\mu_v} e^{-\tau/\mu_s} \rho_s + \rho_s \\ &\left[ \left[ e^{-\tau/\mu_v} t_d(\mu_s) \bar{\rho}^* + e^{-\tau/\mu_s} t_d(\mu_v) \bar{\rho}'^* + t_d(\mu_s) t_d(\mu_v) \bar{\bar{\rho}}^* \right. \right. \\ &\left. \left. + \rho_s \frac{(e^{-\tau/\mu_s} + t_d(\mu_s))(e^{-\tau/\mu_v} + t_d(\mu_v)) S(\bar{\bar{\rho}}^*)^2}{1 - S\bar{\bar{\rho}}} \right] \right] \end{aligned} \quad (5)$$

with

$$\bar{\rho}^* = \frac{\bar{\rho}}{\rho_s^m}, \quad \bar{\rho}'^* = \frac{\bar{\rho}'}{\rho_s^m}, \quad \bar{\bar{\rho}}^* = \frac{\bar{\bar{\rho}}}{\rho_s^m} \quad (6)$$

where  $\rho_s^m$  is a predicted (estimated) surface reflectance, for example taken from a BRDF model. In this modified approach, only the shape of the surface BRDF influences the correction process and not the actual magnitude of the estimated surface BRDF, removing a possible bias. The true surface reflectance  $\rho_s$  can then be obtained by solving (5), which is a quadratic equation in  $\rho_s$  [7].

When the surface is Lambertian,  $\bar{\rho}^* = \bar{\rho}'^* = \bar{\bar{\rho}}^* = 1$  and  $\bar{\bar{\rho}} = \rho_s$ . Thus, (5) can be simplified as

$$\rho_{\text{toa}} = \rho_o + \frac{(e^{-\tau/\mu_s} + t_d(\mu_s))(e^{-\tau/\mu_v} + t_d(\mu_v)) \rho_s}{1 - S\rho_s}. \quad (7)$$

In this case,  $\rho_s$  can easily be calculated without a prior estimate of the BRDF.

In this paper, we investigate systematically the accuracy required in the initial BRDF estimate if a given predetermined accuracy is to be achieved in atmospheric correction. The effect of errors made in the initial assumption on the retrieved surface reflectances is demonstrated and quantified, as is the subsequent error in retrieving the coupling terms. The latter are important because they are albedo, a key parameter in weather and climate models.

We have carried out this study using the 6S code [14]. In its forward mode, 6S can calculate the reflectance at the TOA for a given viewing and illumination geometry according to (1). 6S also performs atmospheric correction in its inverse mode. Here we use its atmospheric correction based on the assumption of a Lambertian surface according to (7), which we will call a Lambertian-based atmospheric correction for the purposes of this paper. We have added an atmospheric correction that considers the surface BRDF based on (5) and uses a BRDF model. This method we will call BRDF-based atmospheric correction. The BRDF model used is the semiempirical Ambrals BRDF model (algorithm for MODIS bidirectional reflectance anisotropy of the land surface) [15] that will be used operationally in deriving BRDF's from MODIS multiangular observations [16]. This model is devised for speed in operational applications, and it is driven by only three parameters. However, validation using field-observed data [17] shows that it is well capable of capturing naturally occurring BRDF shapes. Its accuracy in retrieving BRDF and albedo from sparse angular sampling has been extensively studied [18], [19], and its performance is generally found to be comparable to that of other simple BRDF models. Errors are mostly within a 10% margin for reflectance and albedo.

## B. Parameters and Data Used

In this study, we used the forward mode of 6S to calculate TOA reflectances ( $\rho_{\text{toa}}$ ), as are expected from the MODIS and MISR sensors using (1). Only such simulated observation data give full and systematic control over the variety of atmospheric conditions, surface BRDF types, and especially angular sampling distributions to be investigated for a complete study of the surface-atmosphere coupling problem. To make our simulation convincing, the following variations in conditions were applied.

- 1) *Angular Sampling:* We use Xsatview software [20] to simulate the angular distribution of observations for the EOS MODIS and MISR instruments for geographic locations from latitude 60° S (−60°) to latitude 60° N (+60°) in intervals of 15° during a 16-day period around March 12. This sampling was chosen because data from these two instruments will be combined to derive a BRDF and albedo data product with 1-km spatial

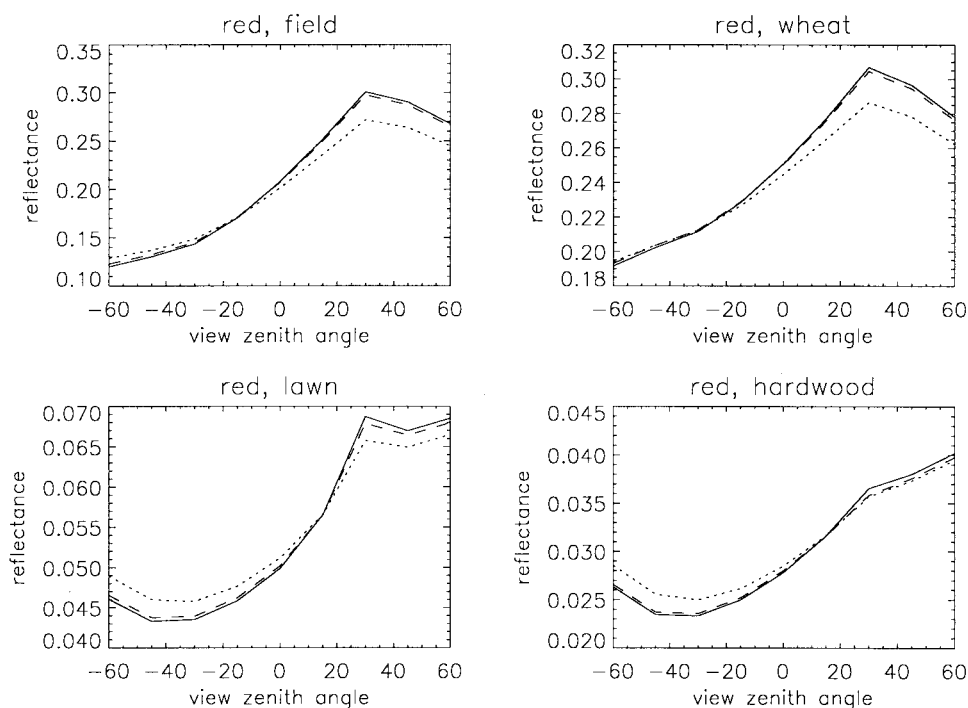


Fig. 1. Red band BRDF in the principal plane (solar zenith angle  $30^\circ$ ) for four different data sets observed by Kimes *et al.* [21], [13], [22]: plowed field, sparse hard wheat, grass lawn, and hardwood forest (representing major land cover types). True value (modeled field observations), solid line; values retrieved from atmospheric correction making the assumption of a Lambertian surface, dotted line; values retrieved from atmospheric correction after one iteration of the surface BRDF-atmosphere coupling loop, dashed line. The aerosol optical depth is 0.2.

resolution for each 16-day period starting in mid-1999 [16]. In the absence of clouds, these two instruments will provide observations in two nearly orthogonal strings across the viewing hemisphere, and, during the time period investigated, for a range of sun zenith angles from  $20$  to  $60^\circ$  [16], [20]. This may be considered relatively good angular sampling; hence, the results found in this study may serve as a baseline for what is possible with good sampling. With reduced sampling [e.g., loss of observations due to clouds, use of MODIS only, MISR only, or the Advanced Very High Resolution Radiometer (AVHRR)] results will be worse accordingly.

- 2) *Surface Cover/BRDF Types*: Four typical land cover types were used in this study, represented by multiangular reflectance data sets observed in the field by Kimes *et al.* [13], [21], [22]. These are a plowed field (barren), a field of hard wheat with only 11% coverage [low leaf area index (LAI)], a grass lawn with a vegetation coverage of 97% (high LAI = 9.9) and a hardwood forest. The semiempirical Ambrals BRDF model [15], [16] was inverted on these data sets to determine model parameters, which were then used to forward-model bidirectional reflectances at the angles given by the respective angular sampling distributions. Both the red and the near-infrared band were studied. Figs. 1 and 2 show the BRDF's of these land cover types, as represented by the Ambrals model, in the principal plane, for a solar zenith angle of  $30^\circ$ , and in the red and near-infrared bands, respectively, as solid lines. As can be seen, these BRDF's cover a variety of

shapes that are typical of most land covers. For example, in the red band, there is a strong hot spot in the surface BRDF of bare soil and the field with sparse vegetation, and an obvious bowl shape with a hot spot for the dense grass lawn and the forest.

- 3) *Atmospheric Conditions*: A continental aerosol model was used to simulate atmospheric conditions. Three aerosol optical depths at a wavelength of 550 nm were employed, 0.1, 0.2, and 0.4. Aerosol optical depth observations (e.g., [23]) show that an optical depth of about 0.1 is typical for semidesert areas (without dust outbreaks) and for land areas in high latitudes ( $>30^\circ$ ); optical depths of about 0.2–0.3 are typical for tropical forest areas during the dry season. Investigations of maximum aerosol optical depths derived from NOAA AVHRR global coverage data show that optical depths over 0.3 are not altogether uncommon, with the highest values occurring over South America and Africa [7].

### C. Magnitude of Atmospheric Effects

To clearly demonstrate the magnitude of atmospheric effects, the root mean square relative errors (rmse's) between the true surface reflectances ( $\rho_s$ ) and those at the TOA ( $\rho_{toa}$ ) are plotted in the top row of panels of Figs. 3 (red band) and 4 (near-infrared band) as a function of latitude and optical depth, and for the four different land cover types. Rmse's were calculated in each instance for the angles given by the respective angular sampling at each latitude. Figs. 5 and 6 show plots of the TOA and at-surface reflectances of the different land cover types in the principal plane in

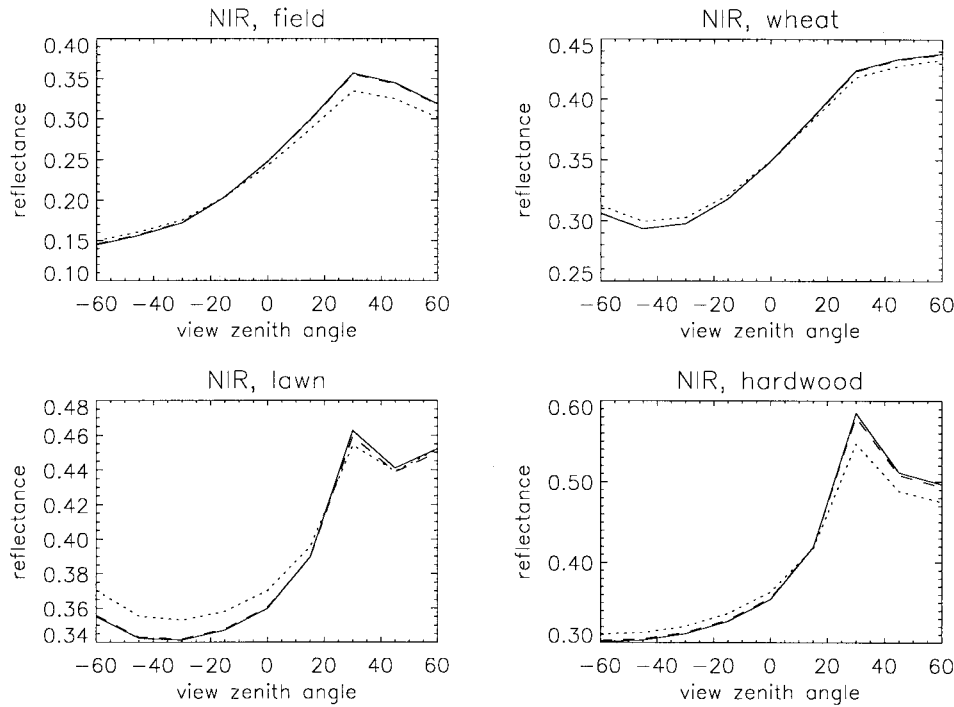


Fig. 2. Near-infrared band BRDF in the principal plane (solar zenith angle  $30^\circ$ ) for four different data sets observed by Kimes *et al.* [21], [13], [22]: plowed field, sparse hard wheat, grass lawn, and hardwood forest (representing major land cover types). True value (modeled field observations), solid line; values retrieved from atmospheric correction making the assumption of a Lambertian surface, dotted line; values retrieved from atmospheric correction after one iteration of the surface BRDF-atmosphere coupling loop, dashed line. The aerosol optical depth is 0.2.

the red and near-infrared bands, respectively, to display how atmospheric scattering affects the shape of the surface BRDF. From these figures, we may see that 1) the atmospheric effects are larger in the red band than in the near-infrared band because atmospheric scattering decreases as wavelength increases and the effect of the atmospheric path radiance is larger relative to the small reflectances of vegetated land covers in the red band than to their larger reflectances in the near-infrared band, and 2) the atmospheric effects increase with increasing optical depth of aerosols (even for an atmosphere with an aerosol optical depth of 0.1 the atmospheric effect is still large, ranging from 3.0% for the hard wheat field to 124% for the hardwood forest in the red band) and the shape of the surface BRDF at the TOA is far different from that of the true one, due to the effect of atmospheric scattering. These results show that atmospheric effects on remotely sensed observations should be removed in remote-sensing applications in which absolute surface reflectances are needed.

#### IV. SENSITIVITY OF ATMOSPHERICALLY CORRECTED SURFACE REFLECTANCES TO THE BRDF ESTIMATES USED IN THE CORRECTION

From (5), we can see that the surface BRDF influences the TOA reflectance through the terms  $\bar{\rho}^*$ ,  $\bar{\rho}'^*$ , and  $\bar{\bar{\rho}}^*$ . In order to study the interrelationship between atmospheric correction and surface BRDF retrieval, we investigate the sensitivity of the retrieved surface reflectance to these ratios. Assuming that an error occurs in the required initial estimates for the three coupling term ratios, either separately in each term  $\bar{\rho}^*$ ,  $\bar{\rho}'^*$ , and  $\bar{\bar{\rho}}^*$ , or in all three terms simultaneously, we calculate the rmse

between the true surface reflectance and the one retrieved as a function of the magnitude of the error made.

Figs. 7 and 8 show mean values for the red and near-infrared bands, respectively, and for different aerosol optical depths. The  $x$ -axes show an assumed relative error in percent in the estimated value of the coupling term ratio(s), and the  $y$ -axes show the mean relative rmse in percent between the true and the retrieved reflectances caused by these errors. The error bars show the range of the rmse in the various cases investigated (different land cover types and angular sampling distributions). Since in each case the TOA reflectance was calculated from the true surface BRDF, a correct initial estimate leads to a perfect retrieval. Any rmse seen is due alone to errors made in the coupling term ratios.

From these plots, we can see the following.

- 1) Sensitivity of the retrieved surface reflectance is nearly linear to any error occurring in  $\bar{\rho}^*$ ,  $\bar{\rho}'^*$  or  $\bar{\bar{\rho}}^*$ . Tables I and II give the approximate slopes of these error functions for the red and near-infrared bands, respectively.
- 2) Retrieved surface reflectance is more sensitive to errors in  $\bar{\rho}^*$  and  $\bar{\rho}'^*$  than to errors in  $\bar{\bar{\rho}}^*$ . This is because the contributions of the surface hemispherical-directional and directional-hemispherical reflectance to the upward radiance naturally are larger than that of the surface hemispherical-hemispherical reflectance.
- 3) Retrieved surface reflectance is much more sensitive to an error made simultaneously in all three coupling term ratios than to an error made in only one of them. For example, for an aerosol optical depth of 0.2 in the red band, a 10% error in  $\bar{\rho}^*$ ,  $\bar{\rho}'^*$ , or  $\bar{\bar{\rho}}^*$  leads to rms errors

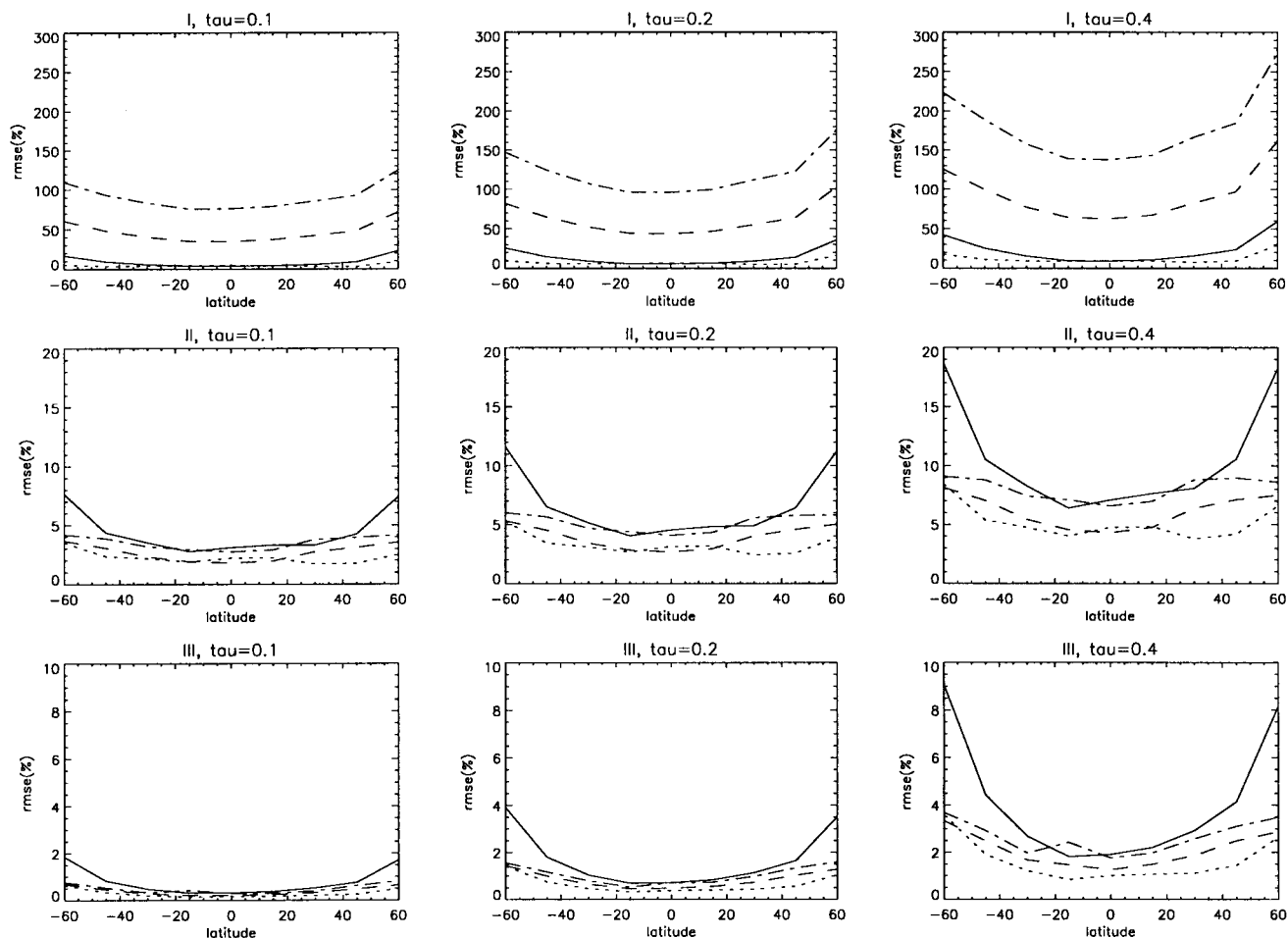


Fig. 3. Red band rms relative errors in percent between the true values of the surface BRDF and the values retrieved from atmospheric correction as a function of latitude for combined MODIS/MISR sampling for a 16-day period around March 12. Plots labeled I (top row) show top-of-atmosphere values, plots labeled II (middle row) show values retrieved from atmospheric correction when making the assumption of a Lambertian surface, and plots labeled III (bottom row) show values retrieved from atmospheric correction after one iteration of the surface BRDF-atmosphere coupling loop. Curves are shown for four different BRDF data sets observed by Kimes *et al.* [21], [13], [22] representing major land cover types: plowed field, solid line; sparse hard wheat, dotted line; grass lawn, dashed line; hardwood forest, dashed-dotted line. In each row, aerosol optical depth increases as indicated from 0.1 to 0.4.

of true to retrieved reflectances of 1–2%. A 10% error in all three terms at the same time, in contrast, leads to an error in the retrieved surface reflectance of about 3%. This case is the more realistic one because, if an approximate BRDF estimate leads to an error in  $\bar{\rho}^*$ , it is very likely that the error will be similar in  $\bar{\rho}'^*$  and  $\bar{\rho}^*$ .

- 4) Sensitivity of the retrieved surface reflectance to errors in the coupling term ratios is larger in the red band than in the near-infrared band and increases as the optical depth of aerosols increases, and the error bars indicate that it varies with land cover type and angular sampling distribution (which influences the angular locations where the reflectances are retrieved).

In the following, we will analyze the relationship between surface BRDF retrieval and atmospheric correction by considering these results in the context of the assumptions commonly made in atmospheric correction models.

#### A. Lambertian-Based Atmospheric Correction

A Lambertian-based atmospheric correction assumes that the surface reflects light isotropically. This is not a very realistic assumption, but it simplifies the problem substantially,

which is why it has been a common assumption in atmospheric correction. In that case,  $\bar{\rho}^*$ ,  $\bar{\rho}'^*$ , and  $\bar{\rho}^*$  are all equal to unity. Since the true values of these coupling ratios are different from unity for the different BRDF types (land cover types) investigated, we may calculate the errors introduced into  $\bar{\rho}^*$ ,  $\bar{\rho}'^*$ , and  $\bar{\rho}^*$  caused by the Lambertian assumption for different aerosol optical depths. Tables I (red band) and II (near-infrared band) show this mean error made for the different land cover types and angular sampling distributions as well as their ranges (in brackets). The error depends on angular sampling because of the normalization of the coupling terms by estimated reflectances defined in (6).

The tables show that errors in the coupling term ratios of more than 10%, in some cases of more than 20%, are implicit in making the Lambertian assumption. For aerosol optical depths of 0.4, errors can be as much as 50%. These numbers, in conjunction with the values of the slope of sensitivity also given, will lead to relevant estimated errors in the atmospherically corrected surface reflectances. For example, the estimated rms relative error in the retrieved surface reflectances is between 1.8 and 7.3%, even for a small aerosol optical depth of 0.1 in the red band.

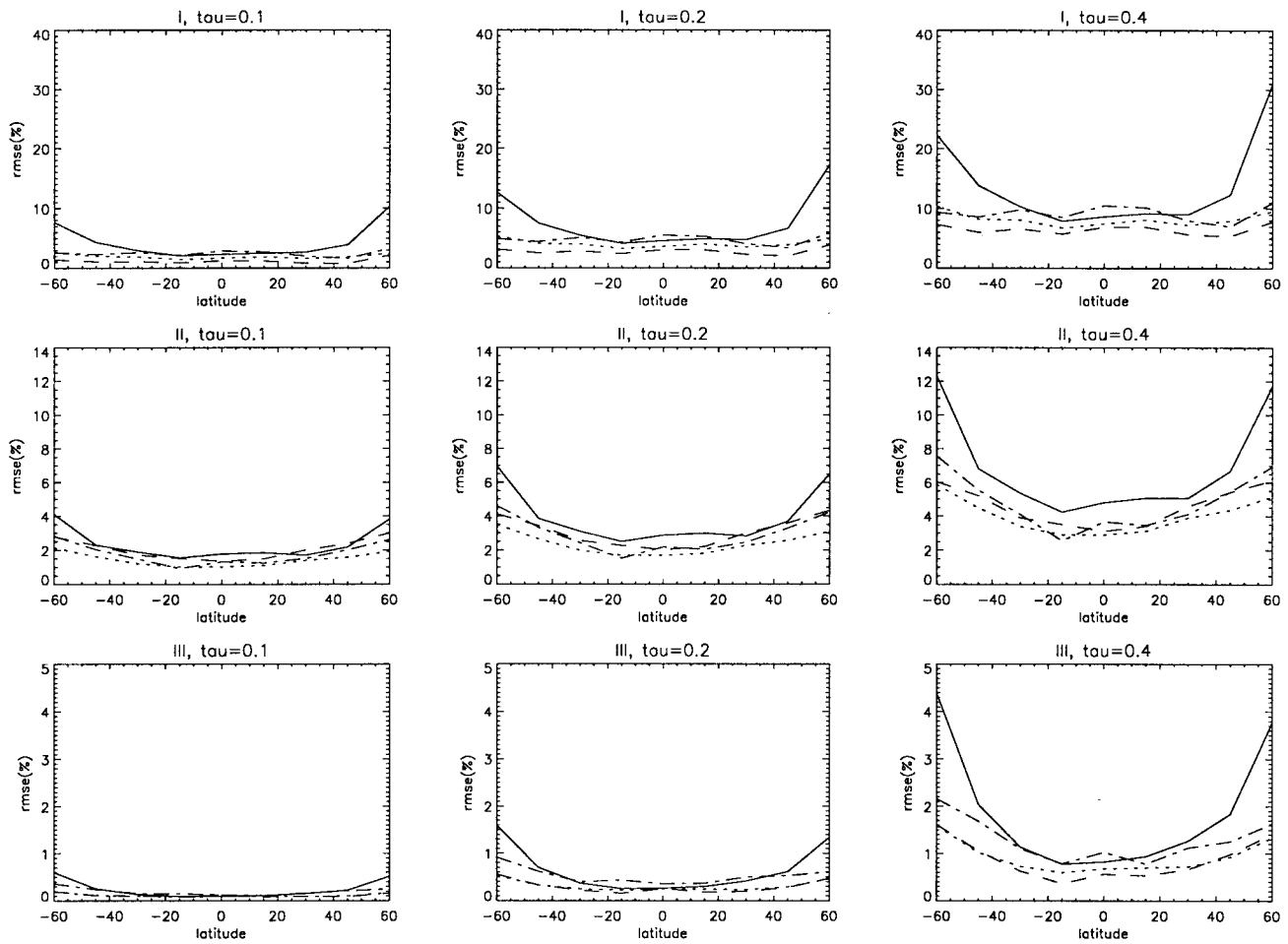


Fig. 4. Near-infrared band rms relative errors in percent between the true values of the surface BRDF and the values retrieved from atmospheric correction as a function of latitude for combined MODIS/MISR sampling for a 16-day period around March 12. Plots labeled I (top row) show top-of-atmosphere values, plots labeled II (middle row) show values retrieved from atmospheric correction when making the assumption of a Lambertian surface, and plots labeled III (bottom row) show values retrieved from atmospheric correction after one iteration of the surface BRDF-atmosphere coupling loop. Curves are shown for four different BRDF data sets observed by Kimes *et al.* [21], [13], [22] representing major land cover types: plowed field, solid line; sparse hard wheat, dotted line; grass lawn, dashed line; hardwood forest, dashed-dotted line. In each row, aerosol optical depth increases as indicated from 0.1 to 0.4.

This can be demonstrated by actually carrying out atmospheric correction based on a Lambertian assumption. TOA reflectances  $\rho_{toa}$  calculated using the inverse mode of 6S were corrected according to (7). Table III shows the mean and range of values (in brackets, for all cases studied) of the relative rmse (in percent) found between the true surface reflectances used in the 6S forward modeling and the surface reflectance values retrieved through atmospheric correction making the Lambertian assumption. As the table shows, even in a nonturbid atmosphere, the error in the retrieved surface reflectance is potentially still a few percent, rather large in view of the accuracies attempted by next-generation sensors like MODIS or MISR. For example, when the aerosol optical depth is 0.1, the mean value of the relative error in the near-infrared is 1.9%, its maximum as high as 4.1%. In the red band, the error increases to a mean value of 3.2% and a maximal value of 7.7%. Furthermore, as the aerosol optical depth increases from 0.1 to 0.4, the mean error increases from 3.2 to 7.5% in the red band and from 1.9 to 5.0% in the near-infrared band, the worst cases having even larger errors.

The large error ranges indicate that the error varies with land cover type and angular samplings, i.e., the BRDF shape. This point is illustrated by the middle row of plots in Figs. 3 and 4. Different land cover types possess different BRDF shapes. Thus, the error caused by the assumption of a Lambertian surface is different. The farther away from isotropy the surface BRDF shapes are, the larger the error is. Among the land cover types used, the plowed field has the strongest anisotropic reflectance characteristics; thus, the error caused for the plowed field is largest. The differences in the error caused in the surface reflectance in different cases became larger with increasing aerosol optical depth.

To see how a Lambertian-based atmospheric correction affects the BRDF shape, we show BRDF plots in the principal plane in Figs. 1 and 2, in which the dotted lines are the BRDF's retrieved from the Lambertian-based atmospheric correction. From these plots, we note that the Lambertian-based atmospheric correction distorts the BRDF shape and that the largest errors occur at the hot spot and bowl edge areas. But the BRDF shapes retrieved from the Lambertian-

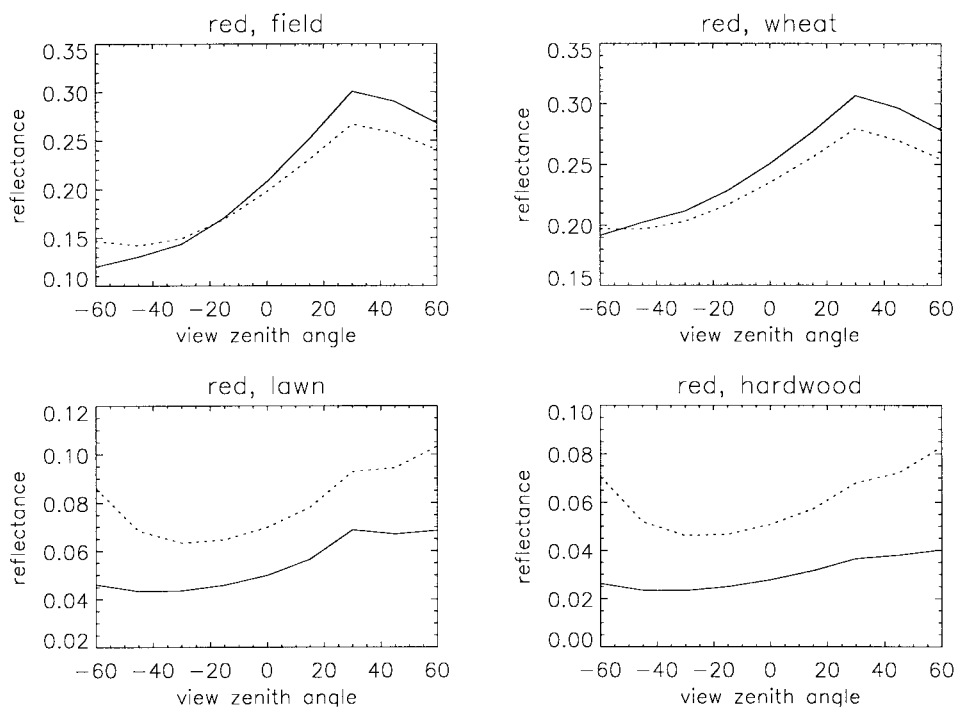


Fig. 5. Red band BRDF in the principal plane (solar zenith angle  $30^\circ$ ) for four different data sets observed by Kimes *et al.* [21], [13], [22]: plowed field, sparse hard wheat, grass lawn, and hardwood forest (representing major land cover types). Surface values (modeled field observations), solid line; top-of-atmosphere values, dotted line. The aerosol optical depth is 0.2.

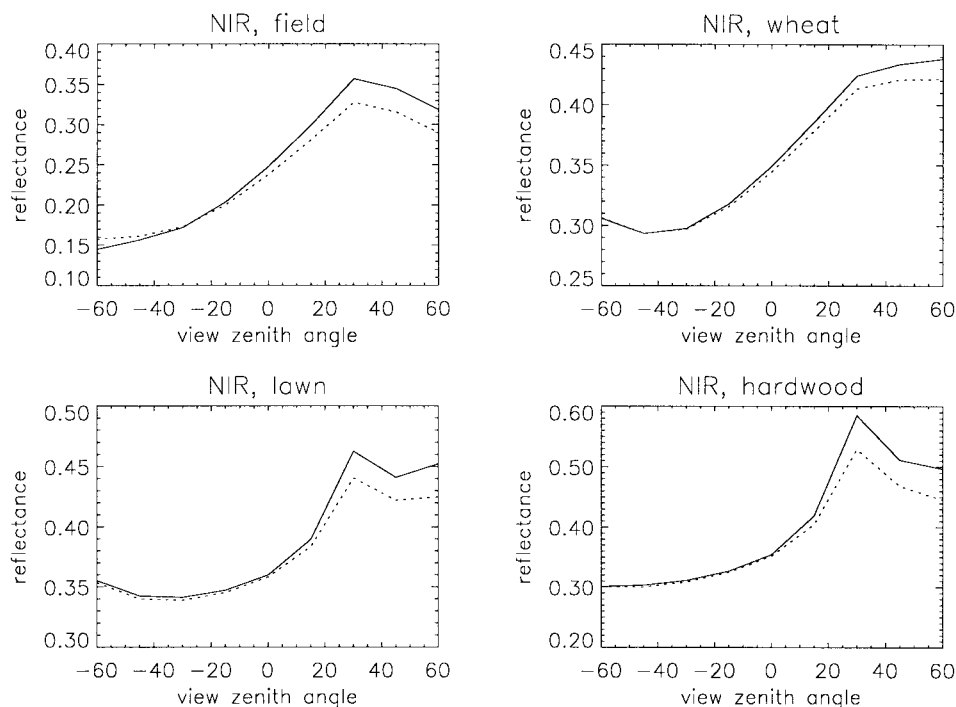


Fig. 6. Near-infrared band BRDF in the principal plane (solar zenith angle  $30^\circ$ ) for four different data sets observed by Kimes *et al.* [21], [13], [22]: plowed field, sparse hard wheat, grass lawn, and hardwood forest (representing major land cover types). Surface values (modeled field observations), solid line; top-of-atmosphere values, dotted line. The aerosol optical depth is 0.2.

based atmospheric correction are nearer to the true ones than an isotropic constant would be.

One direct application of atmospheric correction is to use the retrieved multiangular land surface reflectances to invert a BRDF model that may then be integrated to yield land surface bihemispherical albedo. Table III shows the rmse's found

between modeled and retrieved Ambrals model parameters and bihemispherical albedo. Errors in the retrieved model parameters are very large, displaying mean rmse's such as 13.6% for an aerosol optical depth of 0.1 in the red band, with worst cases showing rmse's of up to 30%. The bihemispherical albedo predicted by the retrieved BRDF model deviates from

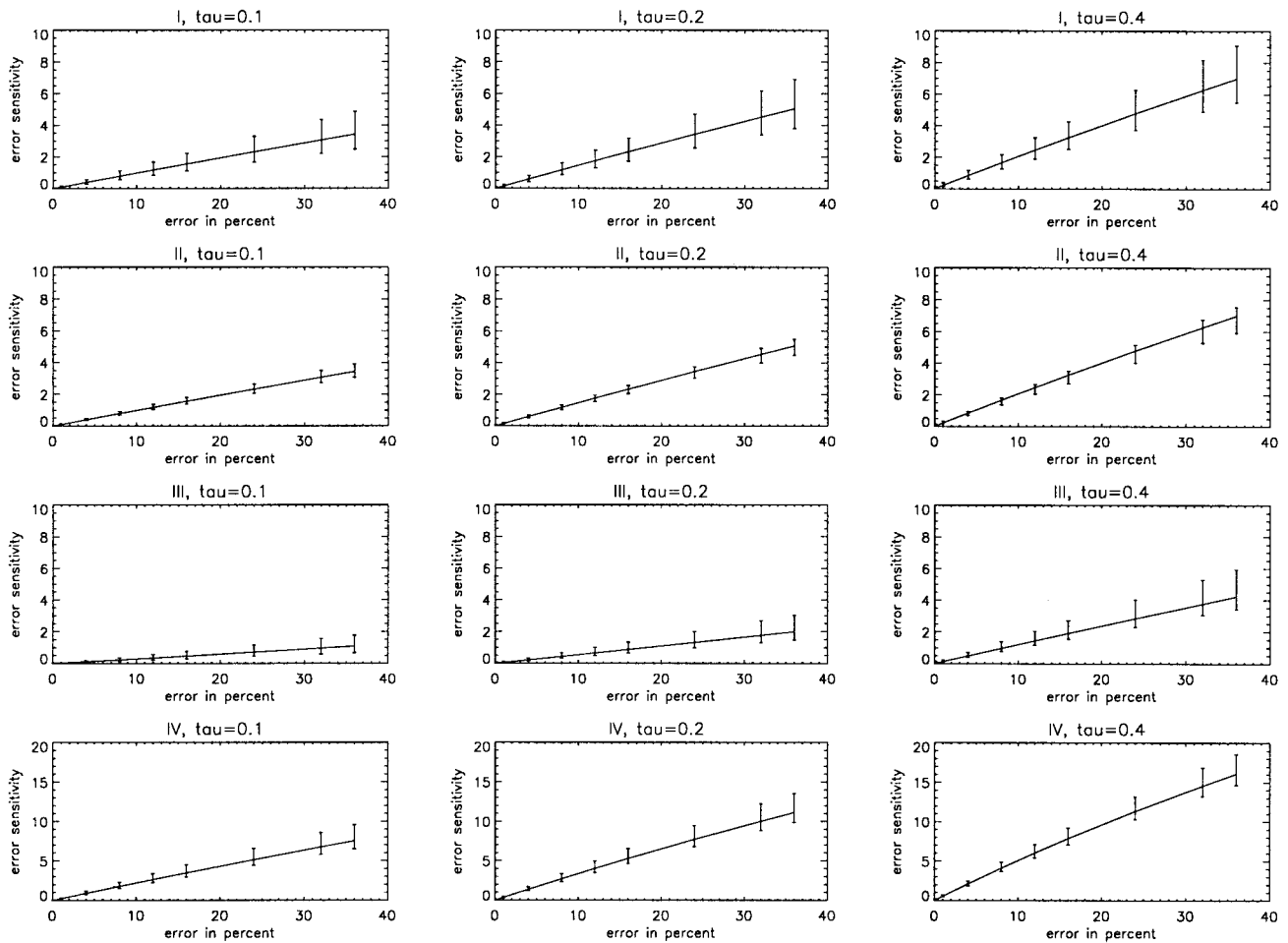


Fig. 7. Red band sensitivity of retrieved surface reflectances to errors in the coupling terms, measured in terms of the rms relative error in percent of the reflectances at the angles observed. Plots labeled I (top row) show the sensitivity to errors in  $\bar{\rho}^*$ , plots labeled II (second row) to errors in  $\bar{\rho}'^*$ , plots labeled III (third row) to errors in  $\bar{\rho}^*$ , and plots labeled IV (bottom row) to errors in all three coupling terms simultaneously. The optical depth increases in each row from left to right from 0.1 to 0.4. Vertical bars show the variation of results with variations of angular sampling with latitude and with land cover type (BRDF type) observed. These plots should be read as follows. Assume an error of a certain size was made in the initial estimate for a coupling term (for example due to making the Lambertian assumption); then the rmse found for the reflectances retrieved from the atmospheric correction can be found from the plot. These retrieved reflectances in turn will allow calculation of a new coupling term with reduced error. We may thus visualize the iterative coupling between surface BRDF and atmospheric correction as an iteration toward the origins of the plots.

its true value by less than 2.0% to almost 5.0% in the red and near-infrared bands for various cases (different latitudes, land cover types, and aerosol optical depths). Depending on the application, this may be an acceptable error. Mean errors are between 1 and 2%. It is not surprising that albedo retrieval is less sensitive to atmospheric correction than BRDF retrieval since it is an integral quality in which reflectances observed at large and small zeniths contribute less than those at intermediate zenith angles. Such conclusions are relevant to data processing for MODIS and MISR, in which BRDF parameters and albedo are among the standard data products.

Generally, these investigations lead to the conclusion that the surface BRDF should be taken into account for accurate retrievals of the surface BRDF. Atmospheric correction based on the Lambertian assumption is not sufficient, especially for aerosol optical depths above or around 0.2.

### B. Atmospheric Correction Using an Iterative Coupling with Surface BRDF Retrieval

If the Lambertian assumption is to be avoided and no reasonably accurate prior knowledge of the BRDF shape

exists, surface BRDF retrieval and atmospheric correction have to be linked. One way to do this is through an iterative loop in which the initial assumption about the BRDF being Lambertian is replaced in the next iteration step by the BRDF retrieved making that assumption. Using this BRDF, improved atmospheric correction yields improved surface reflectances and, thus, a new surface BRDF. This iteration loop may be continued until the desired accuracy is reached. Convergence is assured if the albedos derived from the BRDF model used are approximately correct under the available angular sampling. The BRDF employed in one step will then always yield better results than that used in the previous step.

Here, we investigate whether one cycle of the iteration will already reduce errors to acceptable levels of around 1%. The initial values of  $\bar{\rho}^*$ ,  $\bar{\rho}'^*$ , and  $\bar{\rho}^*$  are estimated from the results of a Lambertian-based atmospheric correction. From the previous calculations, we know that this leads to noticeable errors in the model parameters (Table III). However, the errors caused in  $\bar{\rho}^*$ ,  $\bar{\rho}'^*$ , and  $\bar{\rho}^*$  by using these model parameters are already much smaller. The first iteration then consists of using the Ambrals BRDF model to fit the reflectances

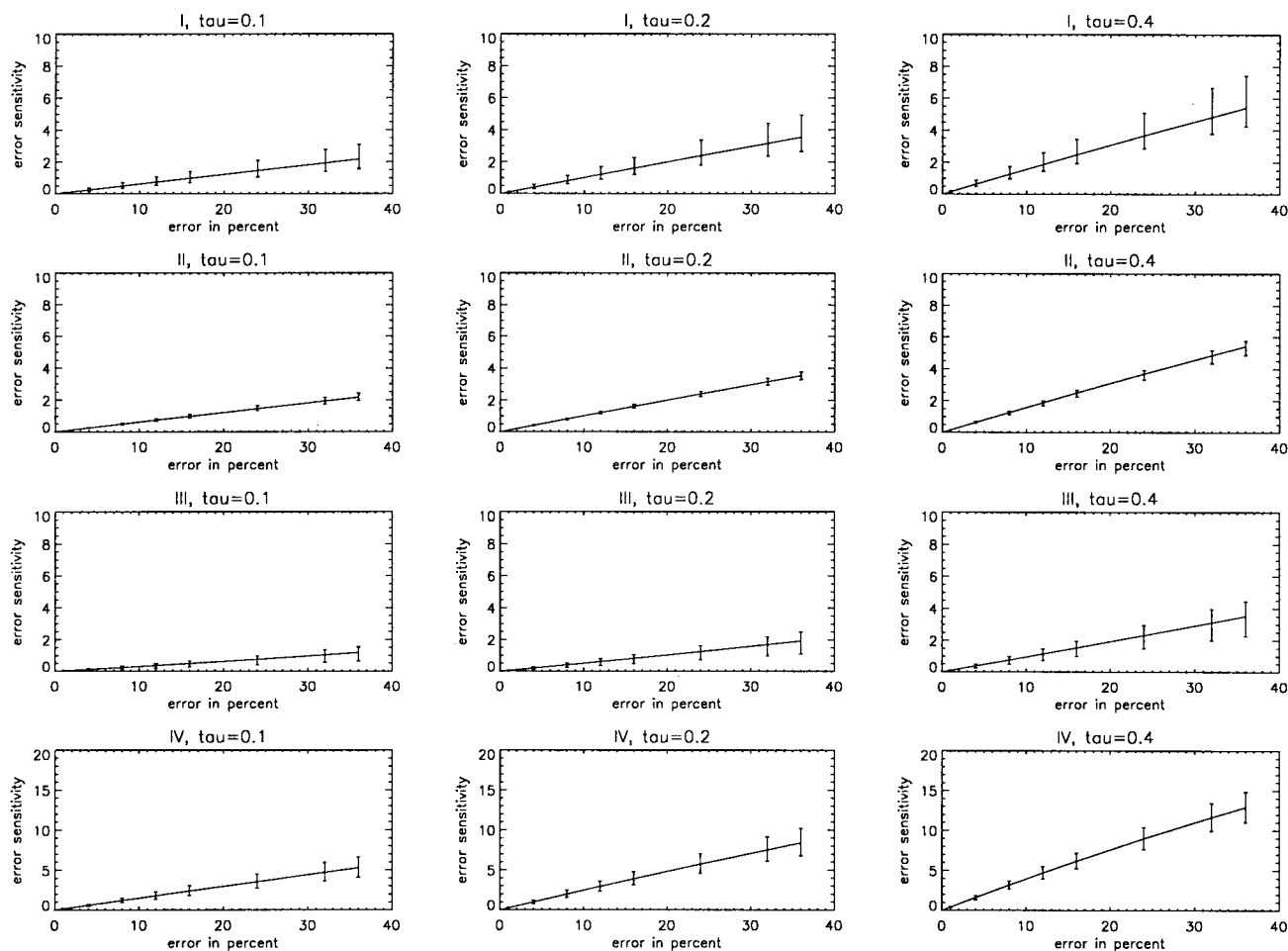


Fig. 8. Near-infrared band sensitivity of retrieved surface reflectances to errors in the coupling terms, measured in terms of the rms relative error in percent of the reflectances at the angles observed. Plots labeled I (top row) show the sensitivity to errors in  $\bar{\rho}^*$ , plots labeled II (second row) to errors in  $\bar{\rho}^{t*}$ , plots labeled III (third row) to errors in  $\bar{\rho}^*$ , and plots labeled IV (bottom row) to errors in all three coupling terms simultaneously. The optical depth increases in each row from left to right from 0.1 to 0.4. Vertical bars show the variation of results with variations of angular sampling with latitude and with land cover type (BRDF type) observed. These plots should be read as follows. Assume an error of a certain size was made in the initial estimate for a coupling term (for example due to making Lambertian assumption); then the rmse found for the reflectances retrieved from the atmospheric correction can be found from the plot. These retrieved reflectances in turn will allow calculation of a new coupling term with reduced error. We may thus visualize the iterative coupling between surface BRDF and atmospheric correction as an iteration toward the origins of the plots.

retrieved from the Lambertian-based atmospheric correction to obtain model parameters, which are then used together with the atmospheric optical parameters to estimate the surface BRDF and  $\bar{\rho}^*$ ,  $\bar{\rho}^{t*}$ , and  $\bar{\rho}^*$  for the subsequent atmospheric correction. This correction we call BRDF retrieval from BRDF-based atmospheric correction.

Tables I and II show the errors between the true  $\bar{\rho}^*$ ,  $\bar{\rho}^{t*}$ , and  $\bar{\rho}^*$  and the values estimated through the one-step atmospheric correction iteration loop. Compared with the errors made when assuming a Lambertian surface, the errors are smaller (2–4% as opposed to more than 10% in the mean), causing smaller errors in the retrieved surface reflectance (refer to the sensitivity slope given). However, when the optical depth of aerosols is large, such as 0.4, the errors in the retrieved surface reflectance are still not less than 1%, as shown in Table IV; in the red band, for example, a mean value of about 2.6% is observed, with the worst case showing errors of up to 9%.

Table IV also shows remaining errors in the BRDF model parameters and surface bihemispherical albedos after performing the first iteration. Compared with the errors caused by

Lambertian-based atmospheric correction (Table III), they are much smaller. In the red band, for example, the mean error in the retrieved surface reflectance decreases from 3.2–7.5% (depending on optical depth) to 0.5–2.6%. The ranges of error are also smaller, which may be seen in the bottom row of plots in Figs. 3 and 4. This is because for each land cover type studied the surface reflectance properties used for the first iteration are nearer to the true ones than those used in Lambertian-based atmospheric correction; thus, the difference in the extent to which the estimated BRDF shapes deviate from the actual ones for different cases is decreased. Retrieved BRDF shapes are shown in Figs. 1 and 2, where the dashed lines are the results found from the first iteration. They are very close to the true values. Bihemispherical albedo errors are also less, down from 1 to 2% to mostly less than 1%.

While errors have been greatly reduced by performing one step of the iteration loop, Table IV still shows errors of several percent in some cases, especially for high aerosol optical depths. We therefore explore the improvements achievable through a second iteration by fitting the Ambrals BRDF

TABLE I

RED BAND MEAN rms RELATIVE ERROR IN PERCENT OF ESTIMATES FOR THE COUPLING TERMS  $\bar{\rho}^*$ ,  $\bar{\rho}'^*$ , AND  $\bar{\rho}^{\#}$  WHEN USING THE LAMBERTIAN ASSUMPTION AND PERFORMING ONE OR TWO ITERATIONS OF ATMOSPHERIC CORRECTION WITH SURFACE BRDF RETRIEVAL (RANGES OF VALUES IN PARENTHESES). MEANS AND RANGES REFER TO DIFFERENT ANGULAR SAMPLING CONDITIONS (MODIS/MISR) AND FOUR DIFFERENT TYPICAL LAND COVER TYPES (BRDF SHAPES). THE SLOPE GIVEN REFERS TO THE IMPACT OF A GIVEN COUPLING TERM ERROR ONTO THE rmse (IN PERCENT) OF THE RETRIEVED BIDIRECTIONAL REFLECTANCES AS COMPARED TO THE TRUE REFLECTANCES

Parameter	Optical Depth	Slope	Lambertian Assumption	BRDF Iteration	
				I	II
$\rho^*$	$\tau = 0.1$	0.10	13.4 (7.1 – 27.7)	2.1 (0.8 – 5.7)	0.3 (0.1 – 0.9)
	$\tau = 0.2$	0.15	12.4 (6.3 – 26.9)	2.8 (1.0 – 7.8)	0.6 (0.7 – 2.0)
	$\tau = 0.4$	0.20	12.0 (6.2 – 27.9)	4.1 (1.5 – 11.8)	1.5 (0.4 – 4.8)
$\rho'^*$	$\tau = 0.1$	0.10	13.4 (7.0 – 28.5)	1.9 (0.6 – 6.0)	0.3 (0.1 – 1.1)
	$\tau = 0.2$	0.15	12.1 (6.0 – 26.8)	2.6 (0.9 – 8.3)	0.6 (0.2 – 2.3)
	$\tau = 0.4$	0.20	11.6 (5.6 – 26.9)	4.0 (1.5 – 12.1)	1.5 (0.5 – 5.3)
$\rho^{\#}$	$\tau = 0.1$	0.03	23.9 (14.3 – 56.5)	3.0 (1.1 – 8.2)	0.4 (0.2 – 1.4)
	$\tau = 0.2$	0.05	23.9 (14.3 – 56.5)	4.2 (1.7 – 12.2)	0.9 (0.4 – 3.0)
	$\tau = 0.4$	0.12	23.9 (14.3 – 56.5)	7.0 (2.8 – 19.0)	2.4 (0.9 – 7.5)

TABLE II

NEAR-INFRARED BAND MEAN rms RELATIVE ERROR IN PERCENT OF ESTIMATES FOR THE COUPLING TERMS  $\bar{\rho}^*$ ,  $\bar{\rho}'^*$ , AND  $\bar{\rho}^{\#}$  WHEN USING THE LAMBERTIAN ASSUMPTION AND PERFORMING ONE OR TWO ITERATIONS OF ATMOSPHERIC CORRECTION WITH SURFACE BRDF RETRIEVAL (RANGES OF VALUES IN PARENTHESES). MEANS AND RANGES REFER TO DIFFERENT ANGULAR SAMPLING CONDITIONS (MODIS/MISR) AND FOUR DIFFERENT TYPICAL LAND COVER TYPES (BRDF SHAPES). THE SLOPE GIVEN REFERS TO THE IMPACT OF A GIVEN COUPLING TERM ERROR ONTO THE rmse (IN PERCENT) OF THE RETRIEVED BIDIRECTIONAL REFLECTANCES AS COMPARED TO THE TRUE REFLECTANCES

Parameter	Optical Depth	Slope	Lambertian Assumption	BRDF Iteration	
				I	II
$\rho^*$	$\tau = 0.1$	0.06	12.6 (7.0 – 23.8)	1.1 (0.5 – 2.9)	0.1 (0.1 – 0.5)
	$\tau = 0.2$	0.10	11.9 (6.6 – 23.7)	1.7 (0.8 – 4.6)	0.3 (0.1 – 1.3)
	$\tau = 0.4$	0.16	11.6 (5.9 – 25.0)	2.7 (1.2 – 7.7)	0.7 (0.3 – 2.0)
$\rho'^*$	$\tau = 0.1$	0.06	11.2 (4.4 – 25.0)	0.9 (0.3 – 3.3)	0.1 (0.1 – 0.3)
	$\tau = 0.2$	0.10	10.3 (4.3 – 24.2)	1.5 (0.4 – 5.2)	0.3 (0.1 – 0.9)
	$\tau = 0.4$	0.16	9.9 (4.3 – 24.5)	2.6 (0.9 – 8.4)	0.7 (0.3 – 2.5)
$\rho^{\#}$	$\tau = 0.1$	0.03	20.5 (11.2 – 55.5)	1.6 (0.6 – 4.6)	0.2 (0.1 – 0.6)
	$\tau = 0.2$	0.05	20.5 (11.2 – 55.5)	2.7 (1.1 – 7.6)	0.5 (0.2 – 1.7)
	$\tau = 0.4$	0.10	20.5 (11.2 – 55.5)	4.5 (1.3 – 12.9)	1.1 (0.5 – 3.5)

TABLE III

RED AND NEAR-INFRARED BAND MEAN rms RELATIVE ERRORS IN PERCENT BETWEEN TRUE BRDF, AMBRALS BRDF MODEL PARAMETERS, AND SURFACE BIHEMISPHERICAL ALBEDO, RESPECTIVELY, AND THEIR RETRIEVED VALUES FROM ATMOSPHERIC CORRECTION WHEN ASSUMING A LAMBERTIAN SURFACE (RANGE OF VALUES FOR DIFFERENT MODIS/MISR ANGULAR SAMPLING DISTRIBUTIONS AND FOUR DIFFERENT TYPICAL LAND COVER TYPES IN PARENTHESES)

Parameter	Band	Optical Depth		
		$\tau = 0.1$	$\tau = 0.2$	$\tau = 0.4$
BRDF	red	3.2 (1.7 – 7.7)	4.7 (2.4 – 11.6)	7.5 (3.8 – 18.3)
	nir	1.9 (0.9 – 4.1)	3.1 (1.5 – 7.0)	5.0 (2.6 – 12.3)
model parameters	red	13.6 (10.4 – 22.5)	17.8 (10.9 – 30.0)	30.2 (24.9 – 41.7)
	nir	8.7 (5.8 – 10.8)	13.3 (9.5 – 20.0)	22.9 (16.7 – 31.4)
bihemispherical albedo	red	1.1 (0.1 – 3.0)	1.5 (0.1 – 3.4)	1.8 (0.2 – 4.9)
	nir	1.5 (0.2 – 2.6)	1.9 (0.4 – 3.0)	2.3 (0.1 – 4.6)

TABLE IV

RED AND NEAR-INFRARED BAND MEAN rms RELATIVE ERRORS IN PERCENT BETWEEN TRUE BRDF, AMBRALS BRDF MODEL PARAMETERS, AND SURFACE BIHEMISPHERICAL ALBEDO, RESPECTIVELY, AND THEIR RETRIEVED VALUES FROM ATMOSPHERIC CORRECTION WHEN PERFORMING ONE ITERATION LOOP BETWEEN ATMOSPHERIC CORRECTION AND SURFACE BRDF RETRIEVAL (RANGE OF VALUES FOR DIFFERENT MODIS/MISR ANGULAR SAMPLING DISTRIBUTIONS AND FOUR DIFFERENT TYPICAL LAND COVER TYPES IN PARENTHESES)

Parameter	Band	Optical Depth		
		$\tau = 0.1$	$\tau = 0.2$	$\tau = 0.4$
BRDF	red	0.5 (0.2 – 1.9)	1.1 (0.3 – 3.9)	2.6 (0.8 – 9.1)
	nir	0.2 (0.1 – 0.6)	0.5 (0.3 – 1.3)	1.3 (0.6 – 1.6)
model parameters	red	1.7 (1.1 – 2.6)	3.7 (2.6 – 5.7)	9.7 (7.0 – 14.5)
	nir	0.7 (0.3 – 1.2)	1.9 (0.9 – 2.8)	5.2 (3.0 – 8.0)
bihemispherical albedo	red	0.4 (0.0 – 0.9)	0.7 (0.0 – 1.7)	1.3 (0.1 – 3.2)
	nir	0.2 (0.0 – 0.3)	0.3 (0.0 – 0.7)	0.7 (0.0 – 1.7)

TABLE V

RED AND NEAR-INFRARED BAND MEAN rms RELATIVE ERRORS IN PERCENT BETWEEN TRUE BRDF, AMBRALS BRDF MODEL PARAMETERS, AND SURFACE BIHEMISPHERICAL ALBEDO, RESPECTIVELY, AND THEIR RETRIEVED VALUES FROM ATMOSPHERIC CORRECTION WHEN PERFORMING TWO ITERATION LOOPS BETWEEN ATMOSPHERIC CORRECTION AND SURFACE BRDF RETRIEVAL (RANGE OF VALUES FOR DIFFERENT MODIS/MISR ANGULAR SAMPLING DISTRIBUTIONS AND FOUR DIFFERENT TYPICAL LAND COVER TYPES IN PARENTHESES)

Parameter	Band	Optical Depth		
		$\tau = 0.1$	$\tau = 0.2$	$\tau = 0.4$
BRDF	red	0.1 (0.0 – 0.3)	0.2 (0.1 – 1.0)	0.9 (0.3 – 3.6)
	nir	0.0 (0.0 – 0.1)	0.1 (0.0 – 0.3)	0.3 (0.1 – 1.2)
model parameters	red	0.2 (0.1 – 0.5)	0.8 (0.4 – 1.1)	3.3 (2.0 – 8.1)
	nir	0.1 (0.0 – 0.1)	0.3 (0.1 – 0.4)	1.3 (0.6 – 2.2)
bihemispherical albedo	red	0.1 (0.0 – 0.2)	0.2 (0.0 – 0.4)	0.5 (0.0 – 1.4)
	nir	0.0 (0.0 – 0.0)	0.1 (0.0 – 0.1)	0.2 (0.0 – 0.9)

are smaller than those occurring after the first iteration, as can be seen from Tables I, II, and V. The mean errors in  $\bar{\rho}^*$ ,  $\bar{\rho}'^*$ , and  $\bar{\rho}^{\#}$  decrease from 4 to 7% in the first iteration to 1 to 2% in the second iteration for an atmosphere with an aerosol optical depth of 0.4 and in the red band. Correspondingly, the mean errors in the retrieved surface reflectances decrease from 2.6 to 0.9%. The errors caused in the model parameters and surface bihemispherical albedos also decrease further. However, the error ranges in the retrieved surface reflectances tell us that, for certain extreme cases, the error of the retrieved surface reflectances may still be a few percent, as for the plowed field, where it is 3.6% in the red band. Depending on the land cover types and the angular sampling available, the iteration loop may need to be performed more than two times in these particular cases. However, generally one or two iterations seem to be completely sufficient for the angular sampling distributions and BRDF types investigated here.

If multiple iterations are to be performed, the question of the speed of convergence arises. To investigate this, we iteratively carried out the loop several times for an aerosol optical depth of 0.4. In each step, we used the Ambrals BRDF model to fit the reflectances retrieved from the previous step and performed a BRDF-based atmospheric correction using the inversion results. The rmse between the true surface reflectances and the retrieved values, and the relative change in the model parameters between subsequent steps, decreases as more iterations are performed. After five iterations, for

models to the surface reflectances retrieved from the first iteration. Because the errors in the model parameters inverted from the first iteration are much smaller than those from the Lambertian-based atmospheric correction, in this step, the errors in  $\bar{\rho}^*$ ,  $\bar{\rho}'^*$ , and  $\bar{\rho}^{\#}$  calculated based on these model parameters should be smaller than those in the first iteration. Consequently, the errors in the retrieved surface reflectances

TABLE VI

RED AND NEAR-INFRARED BAND MEAN RMS RELATIVE ERRORS IN PERCENT BETWEEN TRUE VALUES OF THE COUPLING TERM  $\bar{\rho}^*$  AND ITS VALUE ESTIMATED AFTER PERFORMING ONE ITERATION LOOP BETWEEN ATMOSPHERIC CORRECTION AND SURFACE BRDF RETRIEVAL UNDER THE ASSUMPTION OF AN ISOTROPIC SKYLIGHT DISTRIBUTION (RANGE OF VALUES FOR DIFFERENT MODIS/MISR ANGULAR SAMPLING DISTRIBUTIONS AND FOUR DIFFERENT TYPICAL LAND COVER TYPES IN PARENTHESES). COMPARE TO VALUES IN TABLES I AND II

Band	Optical Depth		
	$\tau = 0.1$	$\tau = 0.2$	$\tau = 0.4$
red	49.2 (5.2 – 16.0)	8.5 (4.3 – 15.8)	7.2 (3.5 – 12.3)
nir	10.0 (3.5 – 17.6)	9.3 (2.6 – 16.3)	8.2 (2.0 – 5.6)

example, the relative change in the model parameters has already decreased to 0.5% and the mean rms error in the retrieved surface reflectances to 0.05% in the red band. The convergence of the iteration loop is found to be more rapid in the near-infrared band than in the red band.

In summary, surface BRDF retrieval and atmospheric correction can be coupled in a converging iteration loop, which may be utilized to improve the quality of atmospheric correction of reflectances and, consequently, the quality of retrieved BRDF's, BRDF model parameters, and bihemispherical albedo.

### C. Effect of Diffuse Skylight on Atmospheric Correction

Equation (2) demonstrates that to know  $\bar{\rho}$  requires knowledge of the downward radiance distribution. Thus, in a BRDF-based atmospheric correction, the exact distribution of skylight needs to be known. Here we will investigate the assumption that the skylight is isotropic, which if reasonable would allow us to be saved from a large amount of calculations. We use the model parameters retrieved from Lambertian-based atmospheric correction and assume the skylight is isotropic to calculate the estimated  $\bar{\rho}^*$ . Table VI lists the mean rmse (and range) between the estimated  $\bar{\rho}^*$  and the true values. Compared with the corresponding results in Tables I and II, where the diffuse skylight distribution is calculated exactly, the estimated error in  $\bar{\rho}^*$  increases from 0.8–5.7% to 5.2–16.0% for an aerosol optical depth of 0.1 in the red band. The corresponding error caused in the surface reflectances by the error in  $\bar{\rho}^*$  increases from 0.1–0.6% to 0.5–1.6%. We therefore conclude that, if accuracies at the percent level are a concern, assumption of an isotropic distribution of skylight should be avoided in atmospheric correction.

### D. Comparison between BRDF-Based Atmospheric Correction Using Absolute Surface BRDF and Using BRDF Shape Only

The atmospheric correction procedure used here normalizes the coupling terms by the values of the estimated bidirectional reflectance in each direction considered [6], [7]. Thus, only the estimated BRDF shape is influencing the correction, not the magnitude of the BRDF. This, it is argued, retains the value of the surface reflectance that is to be retrieved through atmospheric correction as a free variable that is not biased by the BRDF estimate used in the coupling. We investigate whether this actually reduces error in the intended way.

Results for the bihemispherical coupling term are already available. Tables I and III show the rmse between the true

TABLE VII

RED BAND MEAN RMS RELATIVE ERRORS IN PERCENT BETWEEN TRUE VALUES OF THE NONNORMALIZED COUPLING TERMS  $\bar{\rho}$  AND  $\bar{\rho}'$  AND THEIR VALUES ESTIMATED AFTER PERFORMING ONE ITERATION LOOP BETWEEN ATMOSPHERIC CORRECTION AND SURFACE BRDF RETRIEVAL (RANGE OF VALUES FOR DIFFERENT MODIS/MISR ANGULAR SAMPLING DISTRIBUTIONS AND FOUR DIFFERENT TYPICAL LAND COVER TYPES IN PARENTHESES). COMPARE TO VALUES FOR ATMOSPHERIC CORRECTION USING ONLY BRDF SHAPE (TABLE I)

Parameter	Optical Depth		
	$\tau = 0.1$	$\tau = 0.2$	$\tau = 0.4$
$\bar{\rho}$	1.8 (0.8 – 4.6)	2.6 (1.3 – 5.2)	3.9 (2.2 – 8.1)
$\bar{\rho}'$	1.7 (0.8 – 4.4)	2.5 (1.3 – 5.0)	3.8 (2.2 – 7.9)

ratio of the surface bihemispherical albedo to its bidirectional reflectance,  $\bar{\rho}^*$ , and the estimated ratio from the results of the Lambertian-based atmospheric correction, and that between the true surface bihemispherical albedo  $\bar{\rho}$  and its estimated value from the results of the Lambertian-based atmospheric correction, respectively. From these results, we can see that the rmse in  $\bar{\rho}$  is smaller than that in  $\bar{\rho}^*$ . Similarly, we also calculate the estimated errors in  $\bar{\rho}$  and  $\bar{\rho}'$  for the first step of the iteration loop. The results are shown in Table VII. Comparison with the respective entries of Table I reveals that the errors in  $\bar{\rho}$  and  $\bar{\rho}'$  are also smaller than those in  $\bar{\rho}^*$  and  $\bar{\rho}'^*$ . That is to say, not performing the normalization leads to smaller errors in the coupling terms for the cases tested here.

But these coupling terms themselves are just a means for atmospheric correction and surface reflectance retrieval. So the real question is whether atmospheric correction based on (5) is better than that based on (1). To answer this question, we analyze the sensitivity of the retrieved surface reflectance to  $\bar{\rho}$ ,  $\bar{\rho}'$ , and  $\bar{\rho}$  according to (1) under the same simulation conditions as those in the earlier sensitivity analysis. Fig. 9 displays the results for the red band. Comparing Figs. 9 and 7, we can see that the surface reflectance is clearly more sensitive to  $\bar{\rho}$ ,  $\bar{\rho}'$ , and  $\bar{\rho}$  than to  $\bar{\rho}^*$ ,  $\bar{\rho}'^*$ , and  $\bar{\rho}^*$ , especially for large optical depths. Thus, even though the estimated errors in  $\bar{\rho}$ ,  $\bar{\rho}'$ , and  $\bar{\rho}$  are smaller than those in  $\bar{\rho}^*$ ,  $\bar{\rho}'^*$ , and  $\bar{\rho}^*$ , the error caused in the surface reflectances is larger when using coupling terms not normalized by the BRDF magnitude in each direction. BRDF-based atmospheric correction using the estimated surface BRDF shapes alone is better than that using absolute surface BRDF.

### E. Application To Satellite Data

Fig. 10 demonstrates the changes incurred in retrieved reflectance and albedo for five different pixels of NOAA-14 AVHRR data. Data with 1-km spatial resolution were acquired for these five different New England locations during a 16-day period in September 1995. Angular sampling is sparser than for the MODIS-MISR sensor combination, leading to an additional sensitivity of the retrieved reflectances and albedos to changes in atmospheric correction. As may be seen, reflectances at some view zenith angles change considerably and albedo is altered by several percent when performing a one-loop iteration as opposed to making the Lambertian assumption. Unfortunately, no ground-based spectral validation of these findings is currently possible at the required spatial scale and with the necessary accuracy.

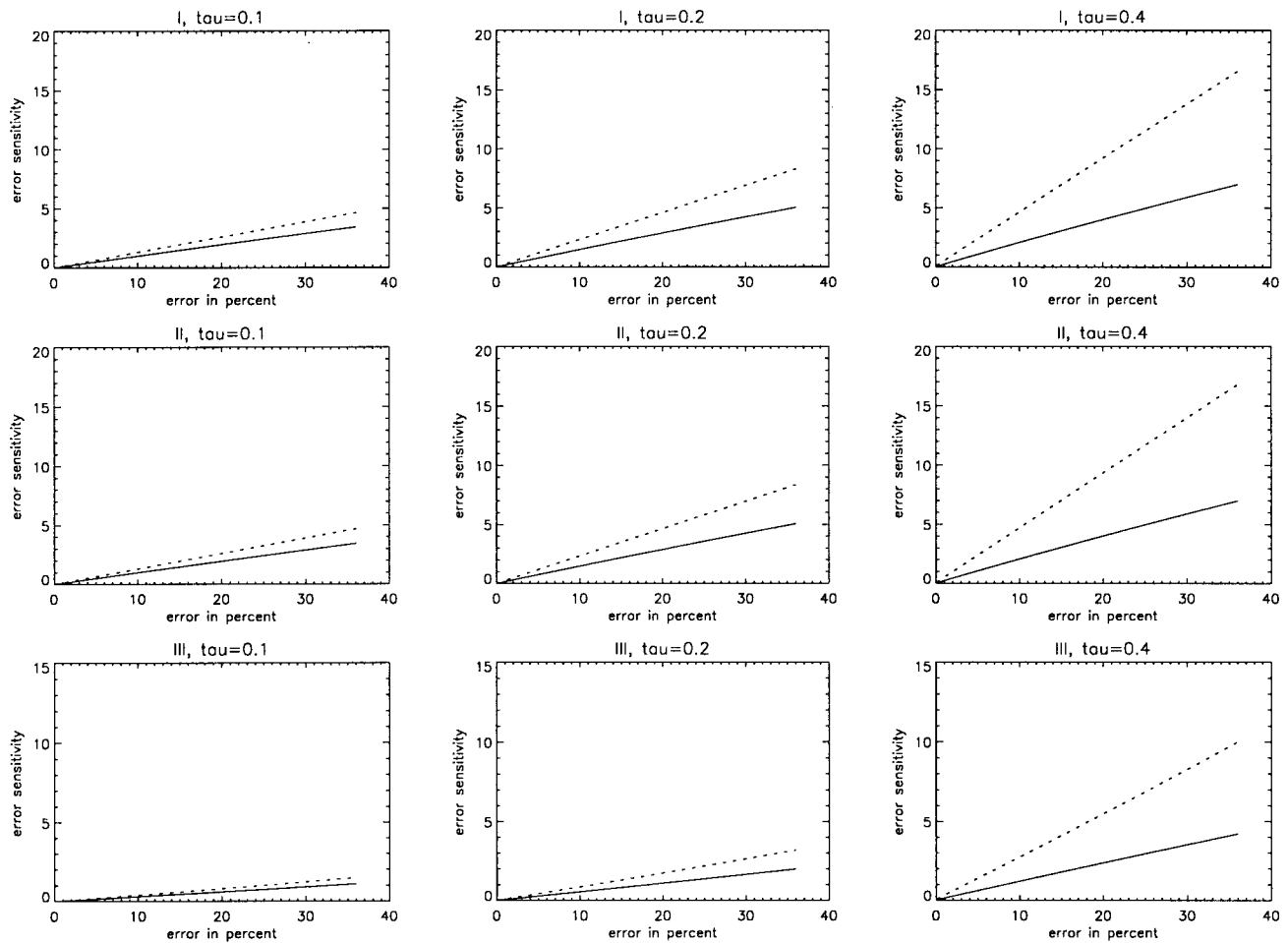


Fig. 9. Red band sensitivity of retrieved surface reflectances to errors in the coupling terms, measured in terms of the rms relative error in percent of the reflectances at the angles observed. The solid lines show the sensitivity when normalizing the coupling terms to the respective bidirectional reflectances, i.e., using only BRDF shape, not magnitude in the atmospheric correction coupling. The dotted lines show the sensitivity when the coupling terms are not normalized. Plots labeled I (top row) show the sensitivity to errors in  $\bar{\rho}^*$ ,  $\bar{\rho}$ ; plots labeled II (middle row) to errors in  $\bar{\rho}^{l*}$ ,  $\bar{\rho}^l$ ; and plots labeled III (bottom row) to errors in  $\bar{\rho}^*$ ,  $\bar{\rho}$ . The optical depth increases in each row from left to right from 0.1 to 0.4.

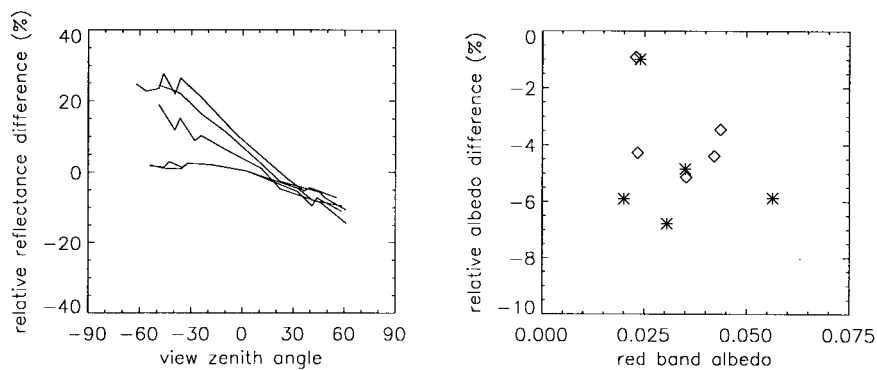


Fig. 10. Comparison of reflectance and albedo retrievals using NOAA-14 AVHRR red band data for a 16-day period in September 1995. Results are shown for five pixels taken over New England: two of a vegetated urban fringe region southeast of Boston, one of the southern borderline between New Hampshire and Vermont, likely forested, and two of the vegetated regions along the Maine coast. Pixels were selected randomly among locations with a maximal number of clear-sky observations during the period (10, 11, or 12 looks, respectively). The left panel shows, as a function of view zenith angle, the relative difference between reflectances retrieved from atmospheric correction when making the Lambertian assumption and when performing a one-iteration loop. The right panel shows the relative error in directional-hemispherical albedo (diamonds) at the solar zenith angle of observation ( $41^\circ$ ) and in bihemispherical albedo (asterisks). Atmospheric correction was performed using surface visibility data from meteorological stations in the area.

### F. BRDF-Based Atmospheric Correction in the Absence of Multiangular Data

Figs. 7 and 8 also provide some insight into the problem of atmospheric correction for satellite sensors that do not have multiangular capabilities, such as the nadir-viewing Landsat sensors. If taking the surface BRDF into account in atmospheric correction is important, the question arises of how to obtain such a BRDF if it cannot be deduced from the data themselves through inversion and iterative coupling. One possibility is to apply the BRDF derived from a different sensor system, another is to use land cover type to predict a BRDF. In either case, the BRDF estimated will only roughly approximate the true BRDF. Figs. 7 and 8 allow us to judge how much error is admissible in the coupling terms derived from the estimated BRDF if the retrieved reflectances are to be within a given error range. The sensitivity curves given indicate that an error of several percent will still lead to an improvement in the correction over making the Lambertian assumption, allowing us to work with estimates that may not be directly derived from the data in question themselves. The caveat here is that the numbers given refer to MODIS/MISR angular sampling distributions, but results for other samplings should be similar.

## V. CONCLUSIONS

In this study, we analyze the sensitivity of atmospherically corrected reflectances to effects of surface anisotropy, as expressed by the surface BRDF and integrals of it. The common simplifying practice of not taking into account surface BRDF effects in atmospheric correction but rather assuming a Lambertian surface is shown to result in mean errors of 3–7% in the red and 2–5% in the near-infrared (depending on optical depth), with worst cases showing errors of up to 10–20% (values given for the range of MODIS/MISR angular sampling distributions and land cover types studied). The farther away from isotropy the BRDF shape is, and the larger the aerosol optical depth, the larger the error becomes. Albedo errors are between 1 and 2% in the red and near-infrared, with worst cases showing errors of up to 5% (3% even for small optical depths).

To overcome these errors, surface BRDF retrieval and atmospheric correction can be coupled in a converging iteration loop. The initial values of surface reflectance properties to be used in atmospheric correction are derived from atmospheric correction making the assumption of a Lambertian surface. The accuracy of the estimated surface reflectance properties used in atmospheric correction then increases as more iterations are performed, and, consequently, the error in the retrieved surface reflectances decreases. One or two iterations are already sufficient to obtain a small mean error: after one iteration, the mean reflectance error is reduced to less than 3% in the red and about 1% in the near-infrared (with worst cases still ranging to several percent more) even for a large atmospheric optical depth of 0.4. After two iterations, the mean errors are below 1% in both bands, with worst cases ranging to not more than about 4% in the red and 1% in the near-infrared, again for optical depth 0.4. Mean bihemispherical albedo errors are

down to about 1% after one iteration (worst cases 3%) for all optical depths, and down to less than about 1% even for the worst cases after two iterations in both bands.

All error values in this study are based on the assumption that the exact atmospheric optical parameters are known. Since this does not hold in actual applications, we will investigate in future work the effect of uncertainty in atmospheric optical parameters on the sensitivity of atmospheric correction of reflectances to the surface BRDF.

This work shows how advanced multiangular remote-sensing techniques, as will be available for example from MODIS or MISR, may be employed to achieve improved land surface reflectance retrievals and hence improved subsequent retrievals of biophysical parameters. As the capability of sensors increases, so should the properties of the algorithms used. MODIS atmospheric processing, for example, in its full implementation, will include the BRDF coupling discussed here (see [7] for details). This study specifies the impact this coupling will have on accuracies. It may also be used to judge the accuracy required in *a priori* assumptions made for BRDF and/or albedo, for example, based on land cover type, in cases in which no multiangular data are available, but effects of land surface anisotropy are nevertheless to be included in atmospheric correction.

## ACKNOWLEDGMENT

The authors wish to thank X. Li, C. Schaaf, and other members of the MODIS BRDF/albedo team for their support and numerous discussions. They also thank M. Barnsley and K. Morris for providing the Xsatview software for modeling of MODIS/MISR angular sampling.

## REFERENCES

- [1] Y. J. Kaufman, "The atmospheric effect on remote sensing and its correction," in *Theory and Applications of Optical Remote Sensing*. New York: Wiley, 1989, pp. 336–428.
- [2] R. M. Case, F. de Hoffmann, and G. Placzek, *Introduction to the Theory of Neutron Diffusion, Vol. 1*. Los Alamos, CA: Los Alamos Sci. Lab., 1953.
- [3] D. Tanre, C. Deroo, P. Duhaut, M. Herman, J. J. Morcrette, J. Perbos, and P. Y. Deschamps, "Simulation of the satellite signal in the solar spectrum (5S)," Laboratoire d'Optique Atmospherique, University des Sciences et Techniques de Lille, Villeneuve d'Ascq Cedex, France, 1986.
- [4] A. Berk, L. S. Bernstein, and D. C. Robertson, "MODTRAN: A Moderate Resolution Model for LOWTRAN 7," USAF Phillips Lab., Hanscom AFB MA, Tech. Rep. GL-TR-89-0122, 1989.
- [5] R. S. Fraser, R. A. Ferrare, Y. J. Kaufman, B. L. Markham, and S. Mattoo, "Algorithm for atmospheric corrections of aircraft and satellite imagery," *Int. J. Remote Sensing*, vol. 13, pp. 541–557, 1992.
- [6] T. Y. Lee and Y. J. Kaufman, "Non-Lambertian effects in remote sensing of surface reflectance and vegetation index," *IEEE Trans. Geosci. Remote Sensing*, vol. GE-24, pp. 699–708, May 1986.
- [7] E. F. Vermote, N. El Saleous, C. O. Justice, Y. J. Kaufman, J. L. Privette, L. Remer, J. C. Roger, and D. Tanre, "Atmospheric correction of visible to middle infrared EOS-MODIS data over land surface: Background, operational algorithm and validation," *J. Geophys. Res.*, vol. 102, pp. 17 131–17 141, 1997.
- [8] S. A. W. Gerstl and A. Zardecki, "Coupled atmosphere/canopy model for remote sensing of plant reflectance features," *Appl. Opt.*, vol. 24, pp. 94–103, 1985.
- [9] H. Rahman, M. M. Verstraete, and B. Pinty, "Coupled surface-atmosphere reflectance (CSAR) model, 1. Model description and inversion of synthetic data," *J. Geophys. Res.*, vol. 98, pp. 20 779–20 789, 1993.

- [10] J. L. Roujean, M. Leroy, and P. Y. Deschamps, "A bidirectional reflectance model of the Earth's surface for the correction of remote sensing data," *J. Geophys. Res.*, vol. 97, pp. 20455–20468, 1992.
- [11] K. T. Kriebel, "Measured spectral bidirectional reflection properties of four vegetated surfaces," *Appl. Opt.*, vol. 17, pp. 352–259, 1978.
- [12] B. Pinty, M. M. Verstraete, and R. E. Dickinson, "A physical model for predicting bidirectional reflectances over bare soil," *Remote Sens. Environ.*, vol. 27, pp. 273–288, 1989.
- [13] D. S. Kimes, W. W. Newcomb, C. J. Tucker, I. S. Zonneveldt, W. van Wijngaarden, J. de Leeuw, and G. F. Epema, "Directional reflectance factor distributions for cover types of Northern Africa," *Remote Sens. Environ.*, vol. 18, pp. 1–19, 1985.
- [14] E. F. Vermote, D. Tanre, J. L. Deuze, M. Herman, and J. J. Morcrette, "Second simulation of the satellite signal in the solar spectrum (6S), 6S user guide," Version 0, NASA Goddard Space Flight Center, Greenbelt, MD, 1994, p. 183.
- [15] W. Wanner, X. Li, and A. H. Strahler, "On the derivation of kernels for kernel-driven models of bidirectional reflectance," *J. Geophys. Res.*, vol. 100, pp. 21 077–21 089, 1995.
- [16] W. Wanner, A. H. Strahler, B. Hu, X. Li, C. L. Barker Schaaf, P. Lewis, J. P. Muller, and M. J. Barnsley, "Global retrieval of bidirectional reflectance and albedo over land from EOS MODIS and MISR data: Theory and algorithm," *J. Geophys. Res.*, vol. 102, pp. 17 143–17 161, 1997.
- [17] B. Hu, W. Lucht, X. Li, and A. H. Strahler, "Validation of kernel-driven models for global modeling of bidirectional reflectance," *Remote Sens. Environ.*, vol. 62, pp. 201–214, 1997.
- [18] W. Lucht, "Expected retrieval accuracies of bidirectional reflectance and albedo from EOS-MODIS and MISR angular sampling," *J. Geophys. Res.*, vol. 103, pp. 8763–8778, 1998.
- [19] J. L. Privette, T. F. Eck, and D. W. Deering, "Estimating spectral albedo and nadir reflectance through inversion of simple BRDF models with AVHRR/MODIS-like data," *J. Geophys. Res.*, vol. 102, pp. 29 529–29 542, 1997.
- [20] M. J. Barnsley, A. H. Strahler, K. P. Morris, and J. P. Muller, "Sampling the surface bidirectional reflectance distribution function (BRDF): 1. Evaluation of current and future satellite sensors," *Remote Sens. Rev.*, vol. 8, pp. 271–311, 1994.
- [21] D. S. Kimes, A. G. Kerber, and P. J. Sellers, "Dynamics of directional reflectance factor distribution for vegetation canopies," *Appl. Opt.*, vol. 22, pp. 1364–1372, 1983.
- [22] D. S. Kimes, W. W. Newcomb, R. F. Nelson, and J. B. Schutt, "Directional reflectance distributions of a hardwood and a pine forest canopy," *IEEE Trans. Geosci. Remote Sensing*, vol. GE-24, pp. 281–293, Jan. 1986.
- [23] Y. J. Kaufman, A. Gitelson, A. Karnieli, E. Ganor, R. S. Fraser, T. Nakajima, S. Mattoo, and B. N. Holben, "Size distribution and scattering phase function of aerosol particles retrieved from sky brightness measurements," *J. Geophys. Res.*, vol. 100, pp. 10 341–10 356, 1994.



**Wolfgang Lucht** received the M.Sc. and Ph.D. degrees in physics from the University of Kiel, Kiel, Germany, in 1990 and 1993.

From 1994 to 1998 he was a Research Assistant Professor in the Department of Geography and the Center for Remote Sensing, Boston University, Boston, MA. Focusing on the physics of scattering and transport phenomena, he has studied the gravitational interaction of many-body systems through numerical simulations, resonant scattering of interplanetary energetic protons in solar magnetic field turbulence, and the interaction of light with vegetation canopies. He is an Associate Member of the MODIS Science Team, where he was responsible for an algorithm for the operational production of a global 1-km BRDF/albedo data product for MODIS. His research interests include vegetation modeling and its applications in remote sensing. He is currently at the Potsdam Institute for Climate Impact Research in Germany.



**Alan H. Strahler** (M'86) received the B.A. and Ph.D. degrees in geography from The Johns Hopkins University, Baltimore, MD, in 1964 and 1969, respectively.

He is currently a Professor of geography and Researcher in the Center for Remote Sensing, Boston University, Boston, MA. He has held prior academic positions at Hunter College, City University of New York, the University of California, Santa Barbara, and the University of Virginia, Charlottesville. Originally trained as a Biogeographer, he has been actively involved in remote-sensing research since 1978. He has been a Principal Investigator on numerous NASA contracts and grants, and he is currently a member of the Science Team for the EOS MODIS instrument. His primary research interests include spatial modeling and spatial statistics as they apply to remote sensing and in geometric-optical modeling of remotely sensed scenes. He is particularly interested in remote sensing of forests and the inference of vegetation canopy parameters from digital images through invertible models.



**Baoxin Hu** received the B.A. and M.S. degrees in electronics engineering from Tianjin University, Tianjin, China, in 1987 and 1990, and the Ph.D. degree from Boston University, Boston, MA, in 1997.

She is currently with York University, Toronto, Ont., Canada, working on land remote sensing research.